ISSN 0021-3640, JETP Letters, 2019, Vol. 110, No. 9, pp. 585–591. © Pleiades Publishing, Inc., 2019.
Russian Text © The Author(s), 2019, published in Pis'ma v Zhurnal Eksperimental'noi i Teoreticheskoi Fiziki, 2019, Vol. 110, No. 9, pp. 584–590.

CONDENSED MATTER

Effects of Ordering in Fe–*x*Al Alloys

A. M. Balagurov[a], I. A. Bobrikov[a, *], and I. S. Golovin[b]

[a] *Joint Institute for Nuclear Research, Dubna, Moscow region, 141980 Russia*
[b] *National University of Science and Technology MISiS, Moscow, 119049 Russia*
**e-mail: bobrikov@nf.jinr.ru*

Received September 24, 2019; revised September 24, 2019; accepted October 3, 2019

The evolution of the structurally different phases and of the microstructural state of Fe–*x*Al alloys is studied in neutron diffraction experiments performed in the high resolution and continuous temperature scanning modes. It is found that the $D0_3$ phase in a weakly nonequilibrium state of alloys occurring in the doping range from $x \approx 23$ to $x \approx 31$ at % has the form of nanoclusters ($L \approx 100$–800 Å) dispersed within a host material (matrix) such as the disordered (A2) or partially ordered (B2) phase. The B2 $\rightarrow$ $D0_3$ $\rightarrow$ B2 $\rightarrow$ A2 phase transitions are accompanied by a decrease or increase in the lattice parameters of these phases in the course of ordering or disordering of the atomic structure, respectively. In this situation, the lattice parameters of both the matrix and clusters change simultaneously and a high degree of coherence of the crystal lattices of the matrix and clusters is observed.

DOI: 10.1134/S0021364019210057

INTRODUCTION

It is well known that the physical and engineering properties of ordered alloys critically depend on the arrangement of their submicrostructure, i.e., on the microstructure on the atomic level. The characterization of the microstructure by X-ray (synchrotron radiation) or thermal neutron diffraction usually includes the analysis of microstructural parameters such as the size of domains with the long-range crystalline order (in the general case, the distribution of these sizes), the magnitude of microstrains in crystallites, and the type and clearness of the crystallographic texture. For ordered alloys, this set of parameters also involves the morphology of domains with regular atomic arrays (their sizes, shape, and spatial organization) and the degree of ordering in them. The formation of domains with a long-range order strongly depends on the alloying conditions and subsequent heat treatment. As a rule, this leads to a microstructure consisting of antiphase domains or relatively small clusters (<1000 Å) with an ordered atomic structure, which are embedded in a structurally less ordered matrix. The concept of antiphase domains, which can be considered as neighboring regions with the same structure but shifted relative to each other by a certain fraction of the translation vector, was put forward in the 1940s [1]. Usually, just this structure is supposed to exist in ordered alloys (see the classical books [2, 3]). The modern presentation of this concept and the description of diffraction effects related to the existence of antiphase domains can be found in the review [4, p. 376].

A sound concept implying the possibility of formation of another type of microstructure in alloys, namely, in the form of bulk clusters with an ordered arrangement of atoms embedded in a disordered host material, appeared in the 1970s. It is based on the analysis of diffuse X-ray scattering data [5] and transmission electron microscopy data [6, 7]. From the model calculations [8], it follows that regions with a short-range order having the characteristic size $L \approx 20$ Å distributed over the disordered host material first arise upon ordering. In the course of a long-term isothermal annealing, their evolution results in the formation of clusters with a long-range order ($L \geq 200$ Å) from them. Further, antiphase domains can be formed from these clusters in the entire volume of the material. Thus, the microstructure in the form of antiphase domains can be considered as a limiting case of the cluster microstructure.

Note that the concept of structurally ordered clusters in alloys is not strictly defined [9]. The computer simulation of the ordering process predicts the existence of interpenetrating domains with smeared boundaries and complicated topology. In our work, the concept of a cluster is used in the diffraction sense; i.e., the cluster is treated as a connected region with the degree of ordering exceeding that in the host material. A set of such regions can be characterized by a certain size determining an additional (size effect) contribution to the width of diffraction peaks.

Both types of ordering in binary alloys—antiphase domains and disperse clusters—give rise to additional Bragg peaks in diffraction spectra, which are usually

referred to as superstructure peaks. Their intensity is relatively low, since it is determined by the difference between atomic form factors in the case of X-ray diffraction or between the coherent scattering lengths in the case of neutron scattering for the elements of the alloy. As a result, it is difficult to analyze such peaks. The superstructure peaks are characterized by a large width resulting from the size effect. A quantitative analysis of the microstructure of the Fe–27Al alloy was performed in our neutron diffraction studies [10, 11]. It was demonstrated that this alloy in the initial (weakly nonequilibrium) state after casting contains clusters with the ordered $D0_3$ structure dispersedly distributed over the host material having a partially ordered B2 structure. The characteristic cluster size in the initial state is $L \sim 200$ Å and it then increases to about 900 Å after the transition of the sample to the disordered state (at $T > 800$°C) and the subsequent slow cooling, which leads to the formation of a nearly equilibrium state. If the state is far from equilibrium (after quenching), then the clusters of the B2 phase arise in the disordered (A2) host material. In [10], we revealed for the first time an amazing fact that the crystal lattices of the matrix and clusters exhibit a very high degree of coherence (the relative difference between the lattice parameters was at the level of 10^{-6}). This fact does not agree with the well-known observation of a significant (by about 0.01 Å) decrease in the lattice parameter of Fe–Al alloys occurring in the course of structural ordering.

To continue these studies, we carried out neutron diffraction experiments for series of Fe–xAl alloys in a wide range of Al contents x (in units of atomic percent) and performed their quantitative analysis. This made it possible to trace the evolution of the structural and microstructural states of alloys up to $x = 50$ at % and to find the correlation between changes in the crystal lattice and ordering effects in the dispersed clusters. The use of neutron diffraction allowed avoiding the influence of surface and local fluctuations on the observed regularities.

SAMPLES, DETAILS OF EXPERIMENT, AND DATA PROCESSING

The as-cast Fe–xAl samples (10 at % $\le x \le$ 50 at %) were prepared by melting the corresponding mixture of pure Fe and Al in an induction furnace in an argon atmosphere and by the subsequent crystallization in a copper mold. The chemical composition of the ingots was determined using energy dispersive spectroscopy with an accuracy of 0.2%. For the neutron experiments, 4 × 8 × 50-mm parallelepiped samples were cut from ingots. In the employed casting, the ingot cooling rate is about 2000 K/min (at the surface), giving rise to a quasiequilibrium state, which noticeably differs in some cases from the equilibrium state. The latter is achieved by a slow (at a rate of about 2 K/min) cooling in the furnace. Numerous available data suggest that three types of structures can be formed in the as-cast Fe–xAl samples in the concentration range up to $x = 50$ at %: the disordered A2 structure ($Im3m$, $a_{A2} \approx 2.92$ Å), as well as partially, B2 ($Pm3m$, $a_{B2} \approx a_{A2} \approx 2.92$ Å), and completely, $D0_3$ ($Fm3m$, $a_{D0_3} \approx 2a_{A2} \approx 5.84$ Å), ordered structures. The atomic positions in these structural phases are given in [10].

The diffraction spectra were measured using a high-resolution Fourier diffractometer (HRFD) at the IBR-2 pulsed reactor (Joint Institute for Nuclear Research, Dubna) [12]. At the HRFD, the time-of-flight method was used to sweep the diffraction spectrum and a high resolution in the interplanar distance is provided by a fast Fourier chopper. It is possible to toggle between the high-resolution ($\Delta d/d \approx 0.0015$) and high-intensity modes with medium resolution ($\Delta d/d \approx 0.015$). The neutron diffraction patterns measured with a high resolution (the simultaneously measured d_{hkl} values range from 0.6 to 4 Å; the total spectrum acquisition time is 1 h) were used for the precision analysis of the atomic structure and widths (profiles) of diffraction peaks. In the second mode, the necessary statistics are accumulated in about 1 min. They are used for continuous temperature scanning at a rate of 1 to 20 K/min.

In the disordered state (phase A2) of the alloy, its diffraction spectrum contains (main) peaks corresponding to the α-Fe lattice with the Miller indices $h + k + l = 2n$. At the ordering in phase B2, the symmetry of the structure decreases to $Pm3m$, which leads to the appearance of peaks with an arbitrary set of Miller indices. The formation of the $D0_3$ phase changes the symmetry of the structure and doubles the lattice parameter. For this structure, diffraction peaks are divided into three groups (when indexing peaks with respect to the unit cell of the $D0_3$ phase):

(i) main peaks with even Miller indices and $(h + k + l) = 4n$,

(ii) superstructure peaks of the first type with all even (h, k, l),

(iii) superstructure peaks of the second type with all odd (h, k, l).

In addition, the Miller indices for the $D0_3$ phase satisfy the standard selection rules for a face-centered unit cell; i.e., there are no diffraction peaks with indices mixed in parity. For composition $x \approx 25$ at % (Fe_3Al) at low (up to ~500°C) temperatures, the peaks corresponding to all three groups are visible in the diffraction spectra ($D0_3$ phase). Further on (up to 700°C), the peaks of the first two groups remain (B2 phase) and, finally, the peaks of only the first group survive (A2 phase).

The intensities of the main, I_f, and superstructure, I_s, diffraction peaks are characterized by the temperature dependences

$$I_f \sim V_f(T)|F_f|^2 \exp[-W(T)],$$
$$I_s \sim V_s(T)\xi^2(T)|F_s|^2 \exp[-W(T)], \quad (1)$$

where $V_f(T)$ and $V_s(T)$ are the volume fractions occupied by the phase responsible for the corresponding peaks, F_f and F_s are the structure factors for the corresponding peaks, $\xi(T)$ is the factor characterizing the degree of atomic ordering ($0 \le \xi \le 1$), $\exp[-W(T)]$ is the Debye–Waller factor. For brevity, standard Lorentz and absorption factors, as well as the extinction coefficient, are omitted in Eqs. (1). In the case of neutron diffraction by a stoichiometric alloy, e.g., FeAl, with the B2 structure, $F_f = (b_{Fe} + b_{Al})$ and $F_s = (b_{Fe} - b_{Al})$, where $b_{Fe} = 9.45$ fm and $b_{Al} = 3.45$ fm are the neutron coherent scattering lengths for iron and aluminum nuclei, respectively. For the $D0_3$ structure and stoichiometric Fe_3Al composition, we have $F_f = (3b_{Fe} + b_{Al})$ and $F_s = (b_{Fe} - b_{Al})$. Hence, at the complete ordering, i.e., at $\xi = 1$, the structure factors for the main peaks are larger than those for the superstructure ones by a factor of 2.2 and 5.3 for B2 and for $D0_3$ structures, respectively.

In the presence of a long-range ferromagnetic order in the alloy, all diffraction peaks, including superstructure ones, exhibit some magnetic contribution modulated by the magnetic form factor of iron. However, owing to a low ordered magnetic moment of iron ($\mu_{Fe} \le 2\mu_B$), this contribution is small. The examples of diffraction spectra measured with high resolution in various phases of Fe–xAl are shown in Fig. 1.

The profiles of the diffraction peaks measured by the HRFD are primarily determined by the contribution from the Fourier chopper, which is close to a Gaussian one with the width depending on the maximum speed and on the used frequency distribution function of the chopper rotation [12]. In the case of a real crystal, additional broadening arises owing to microstrains in crystallites, ε, and the finite sizes of coherently scattering domains. For the HRFD, the dependence of the width of the diffraction peak on the interplanar distance d is determined by the Williamson–Hall formula

$$(\Delta d)^2 = C_1 + (C_2 + C_3)d^2 + C_4 d^4. \quad (2)$$

Here, C_1 and C_2 the constants related to the diffractometer, $C_3 \approx (2\varepsilon)^2$, $C_4 \approx (k/L)^2$, and k is the Scherrer constant about unity taking into account the shape of coherently scattering domains. In the absence of size effect (large coherently scattering domains) and in the presence of it, the dependence of $(\Delta d)^2$ on d^2 should be linear and parabolic, respectively. Accordingly, this dependence plotted in a sufficiently wide d_{hkl} range makes it possible to determine ε and L. The practice of working with the HRFD has shown that its resolution allows one to reliably determine microstrains at a level of $\varepsilon \approx 0.001$ and the characteristic sizes of coherently scattering domains about $L \approx 2500$ Å and even smaller.

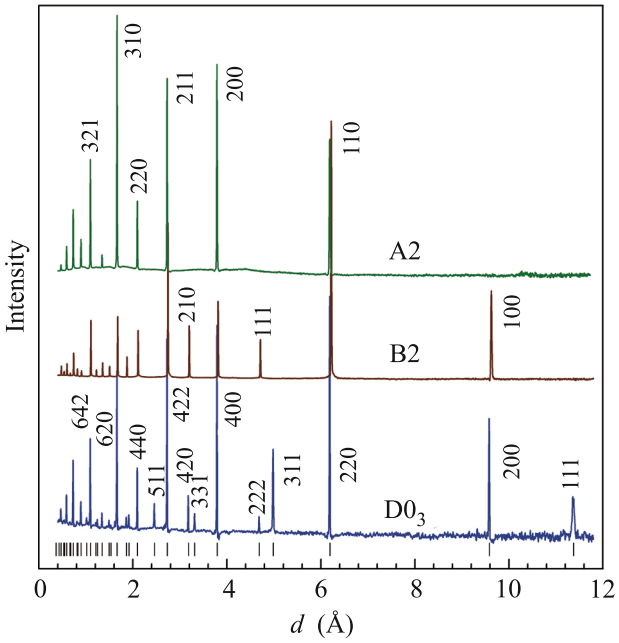

Fig. 1. (Color online) Neutron diffraction spectra of Fe–xAl alloys in (from bottom to top) the $D0_3$ ($x = 27$ at %), B2 ($x = 50$ at %), and A2 ($x = 16$ at %) phases. Vertical dashes indicate the calculated positions of the peaks in the $D0_3$ phase. To pass to the unit cell of this phase, all Miller indices in the A2 and B2 phases should be multiplied by a factor of 2.

In the model of dispersed clusters, which is valid for the cast Fe–xAl samples, as shown in [10], the size effect is determined by the sizes of coherently scattering domains both in the clusters and in the host material, the ratio of which can be arbitrary. Owing to the high symmetry of the crystal lattices, the relatively small lattice parameters, and the high resolution of the HRFD, all measured peaks in the neutron diffraction spectra of Fe–xAl are separated and their main characteristics (intensity, position, and width) can be determined individually for each peak. This property is important for the analysis of the accuracy of the results obtained and makes it possible to independently determine the lattice parameters for the host matrix and clusters and to control the possible effects of anisotropic peak broadening.

RESULTS

According to the presence of certain peaks in the diffraction spectra, cast Fe–xAl alloys with the growth of x are transformed from the disordered A2 phase to the $D0_3$ phase at $x \approx 19$ at % and then to the B2 phase at $x \approx 33$ at %. This was found in the beginning of 1930s [13] and is shown in the well-known phase diagrams (see, e.g., [14]). However, a more detailed study, including the analysis of the widths and intensities of diffraction peaks, leads to a much more complicated picture.

The characteristic dependences of $(\Delta d)^2$ on d^2 for three structurally different phases of Fe–xAl alloys are shown in Fig. 2. In the cases of the A2 and B2 phases, all experimental points are fitted by one parabolic curve, whose coefficients allow determining ε and L. The magnitude of microstrains for all studied alloys appears to be very small ($\varepsilon < 0.001$), and the size of coherently scattering domains varies from 1200 to 2200 Å. This behavior of the peak widths corresponds to a homogeneous structure, although the relatively small size of the coherently scattering domains suggests the existence of a large number of defects. For the alloys with compositions located in the range of existence of the $D0_3$ phase, the situation is different. Indeed, the widths of diffraction peaks as functions of d_{hkl} are fitted by two plots, nearly linear for the peaks allowed in the A2 and B2 phases and parabolic for the superstructure peaks allowed only in the $D0_3$ phase. This picture completely corresponds to the microstructure formed by clusters of the ordered $D0_3$ phase embedded in a partially ordered host material having the B2 structure. For the Fe–27Al poly- and single crystals, the detailed analysis of the diffraction data providing the temperature dependence of the characteristic cluster sizes and the degree of ordering in them was performed in [10, 11]. The $D0_3$ clusters are observed up to $x = 31$ at %, whereas their size decreases to $L \approx 80$ Å.

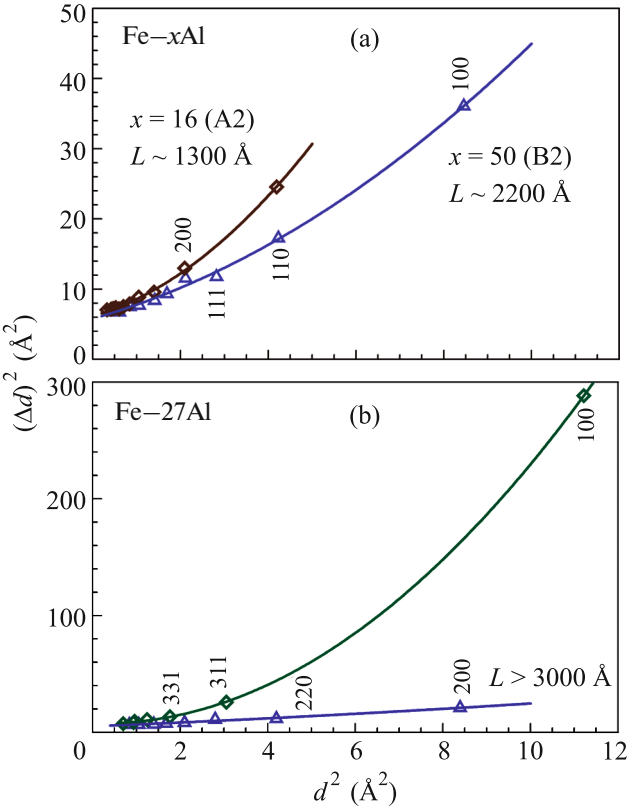

Fig. 2. (Color online) Williamson–Hall plots for the diffraction peaks in Fe–xAl alloys: (a) $x = 16$ at % (A2 phase) and $x = 50$ at % (B2 phase) and (b) $x = 27$ at % ($D0_3$ phase). For $x = 16$ and 50 at %, the curves are parabolic and the characteristic sizes of coherently scattering domains are 1300 and 2200 Å, respectively. For $x = 27$ at %, the plot is nearly linear for the peaks allowed in the A2 and B2 phases ($L > 3000$Å), and it is parabolic for the superstructure peaks allowed in the $D0_3$ phase. The latter plot corresponds to the characteristic size ~700 Å of coherently scattering domains. The values of Δd are multiplied by 10^3.

With an increase in the Al content in alloys, the lattice parameter and the intensities of diffraction peaks evolve (Fig. 3). The observed deviation of the lattice parameter from a linear relationship with the increase in x, i.e., its actual decrease upon transition to an ordered state, is long standing and well known for binary alloys. In particular, for Fe–xAl alloys, the detailed X-ray data are presented in [15], and they coincide with our data with an accuracy of 0.001 Å. The mechanisms of this phenomenon are still under discussion. In particular, in review [16] on the basis of experimental data for a large number of binary alloys, it is discussed whether the decrease in the lattice parameter is related to energy or geometrical (difference in ionic radii) factors. The available data correlate better with a change in the ordering energy and, accordingly, the ab initio calculations can qualitatively predict the observed dependence of the lattice parameter on the composition, as demonstrated in [17] for Fe–Ga alloys.

A surprising issue (which has not attracted attention before) is illustrated in Fig. 3, where the shown lattice parameters are determined by the positions of the main peaks, i.e., by those characteristic of the host material. Since clusters in the initial state of cast samples occupy ≤40% of the sample volume (according to the estimate made in [11]), one could expect that the lattice parameter for the host material would grow linearly with x (as in the A2 phase) at the Al content ranging from $x \approx 23$ at % to $x \approx 31$ at %. In this case, the profiles of the main diffraction peaks in high-resolution spectra would be the sum of narrow peaks from the host material and wide peaks from the clusters, which are shifted relative to each other by $\Delta d \approx 0.01$ Å, but this is not observed. Moreover, as shown in [10], the

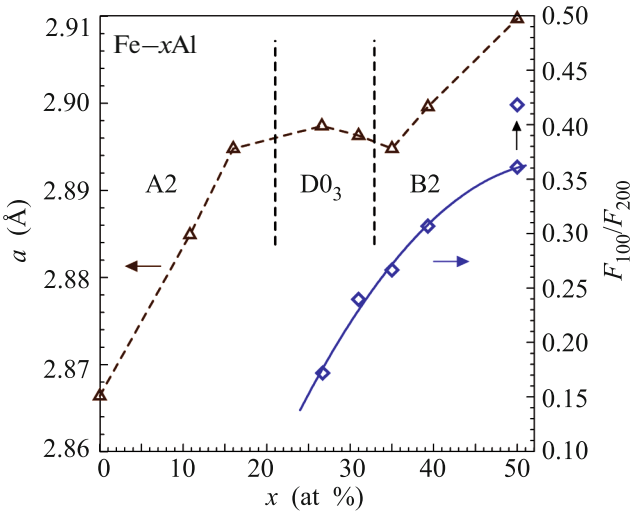

Fig. 3. (Color online) Lattice parameter (for the D0$_3$ phase, we show $a' = a/2$) and the ratio of structure factors for the 100 and 200 reflection orders of the B2 phase versus x. At $x = 50$ at %, we show two points: the lower one corresponds to the cast sample and the upper one describes this sample after its heating and slow cooling (nearly equilibrium state). The vertical lines divide (provisionally) the ranges of existence of the A2, D0$_3$, and B2 phases as the main structural phases. The sizes of the symbols approximately represent the experimental errors.

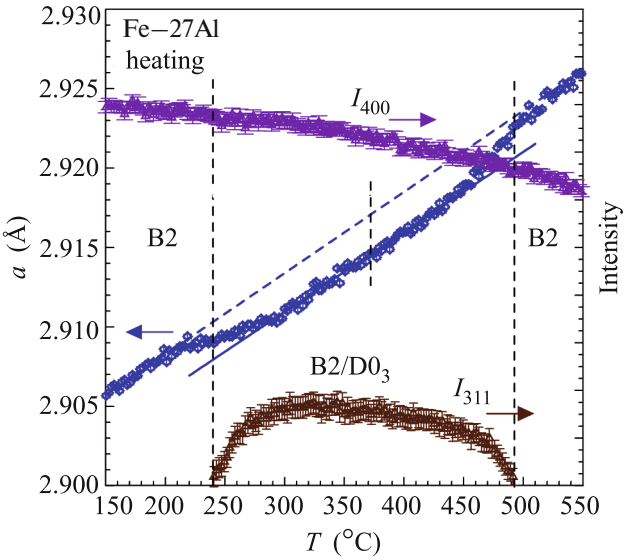

Fig. 4. (Color online) Temperature dependence of the lattice parameter in the host material (B2 phase) and the intensities of the main (I_{400}) and superstructure (I_{311}) peaks of the D0$_3$ phase measured on heating the Fe–27Al alloy. Within the temperature range 240°C < T < 490°C, the microstructure of the sample can be considered as the host material formed by the partially ordered B2 phase with the clusters of the ordered D0$_3$ phase dispersedly distributed over it. The lattice parameter decreases at ordering and increases at disordering. The indicated Miller indices correspond to the unit cell of the D0$_3$ phase.

lattice parameters determined from the positions of separate main and superstructure peaks fall in the range of ±0.0001 Å; i.e., the crystal lattices of the host material and clusters exhibit a very high degree of coherence.

The above discussion is supported by the data on the correlation of the lattice parameter and the ordering in the form of dispersed clusters, which we have obtained for the Fe–27Al alloy remaining in its initial nonequilibrium state on slow heating (2 K/min). In the course of heating the sample, the B2 → D0$_3$ → B2 → A2 phase transformations are detected by appearance and disappearance of the superstructure diffraction peaks. In Fig. 4, we can see that the 311 superstructure peak, related to the formation of clusters of the D0$_3$ phase, arises at $T \approx 240$°C and exists up to $T \approx 490$°C. In the same temperature range, we can observe the characteristic decrease in the lattice parameter determined, as before, from the positions of the main peaks, i.e., for the B2 host material. The intensity of the main peaks decreases smoothly, without any sharp changes, in accordance with the decrease in the Debye–Waller factor. In this case, the effective decrease in the lattice parameter is about 0.0025 Å. Such value is several times smaller than that occurring in the course of varying x apparently because structural ordering in the clusters is incomplete.

The F_{100}/F_{200} structure factor ratio (the ratio is used to eliminate the possible effect of texture on the intensity of peaks) illustrated in Fig. 3 implies that the intensity of superstructure peaks increases gradually with x. For the B2 phase, the calculation of structure factors depending on the Al content and on the degree of ordering gives

$$F_{100}/F_{200} = 2(x - y)\Delta b/(2b_{\mathrm{Fe}} - 2x\Delta b), \qquad (3)$$

where y is the fraction of disordered atoms ($y = 0$ at the highest possible ordering in the alloy at a given x value) and $\Delta b = b_{\mathrm{Fe}} - b_{\mathrm{Al}}$. The measured values of this ratio shown in Fig. 3 are in qualitative agreement with Eq. (3). Quantitative agreement is achieved under the assumption that the structure is incompletely ordered (in the range from 1 to 10%) or that extinction affects the intensities of the clearly pronounced peaks (in the same range).

Changes in the intensities of diffraction peaks upon heating of the samples and the temperature dependences of the structural characteristics deduced from them for the alloy with $x = 27$ at % were discussed in detail in [10]. The new data confirm that the D0$_3$ → B2 → A2 structural transformations observed in Fe–xAl alloys up to $x = 31$ at % are typical second order transitions. Unusual temperature dependences were observed only for the Fe–50Al alloy; namely, the normal decrease in intensities attributed to the Debye–Waller temperature factor is unexpectedly

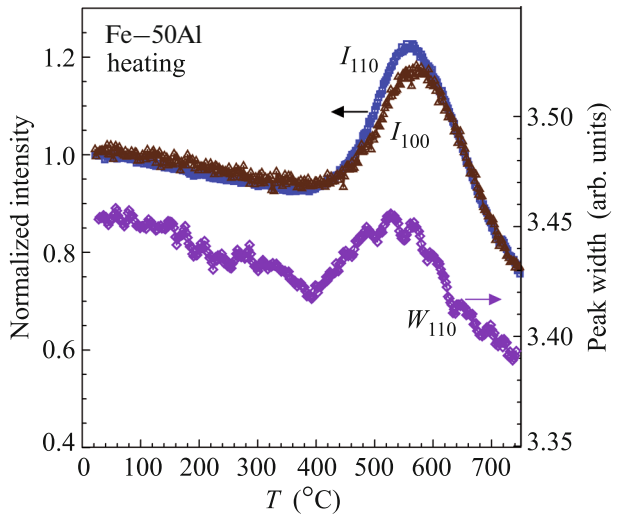

Fig. 5. (Color online) Temperature dependence of (left axis) the normalized intensities of superstructure (I_{100}) and main (I_{110}) peaks and (right axis) the width of the main peak (W_{110}) measured on heating the Fe–50Al alloy at a rate of 2 K/min.

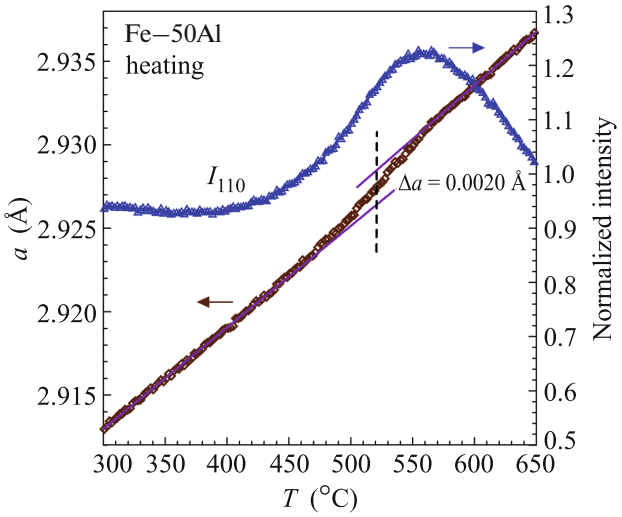

Fig. 6. (Color online) Temperature dependence of (right axis) the normalized intensity of the diffraction peak (I_{100}) and (left axis) the lattice parameter of the B2 phase measured on heating of Fe–50Al alloy.

transformed to a peak arising at $T \approx 550$°C in the intensities of both the main and superstructure peaks (Fig. 5). This effect is most probably caused by extinction; i.e., a noticeable decrease in the long-range order occurs in this temperature range; hence, extinction decreases, increasing intensities. This assumption is indirectly confirmed by the increase in the widths of all diffraction peaks in the same temperature range, which is also shown in Fig. 5.

This assumption is also confirmed by the behavior of the lattice parameter upon heating (Fig. 6). According to its S-shaped change by 0.002 Å near 520°C, the disordering of the structure occurs in the range of 450–570°C; i.e., the degree of ordering in the B2 phase decreases over the entire volume of the sample or in some part of it and the B2 → A2 transition occurs. This should lead to a certain decrease in the intensities of superstructure peaks, but with a strong decrease in the extinction effect, the observed increase in intensities is possible.

CONCLUSIONS

The main results of this work are as follows. Neutron diffraction experiments performed with a high resolution in the interplanar spacing and employing the continuous temperature scanning regime have made it possible to trace the evolution of the structural phases and the microstructural state of Fe–xAl alloys. It has been demonstrated that the cast samples (corresponding to a weakly nonequilibrium state) with the Al content from $x \approx 23$ at % to $x \approx 31$ at % exhibit the formation of nanoclusters ($L \approx 100$–800 Å) dispersedly distributed in the disordered (A2) or partially ordered (B2) host material.

At the temperature scanning, the B2 → $D0_3$ → B2 → A2 transitions are accompanied by the characteristic changes in the temperature dependence of the lattice parameter: its decrease at ordering and increase at disordering. It has been found that the lattice parameters of both the host material and clusters vary synchronously and remain highly coherent. This behavior was previously unknown. The accurate values of the lattice parameters, determined independently from the positions of the main and superstructure peaks, suggest that the difference between the lattice constants of the host material and clusters, if it actually exists, is much less than the expected value (<0.0002 Å).

The ab initio calculations reported in [17] for Fe–xGa alloys demonstrated the possibility of an adequate theoretical interpretation of this effect. The corresponding progress in the calculation technique can make it possible to predict the nucleation of clusters with an ordered structure, to estimate their sizes and the degree of ordering in the domains occupied by the $D0_3$ phase, and to find possible differences between the lattice parameters of the host material and clusters.

ACKNOWLEDGMENTS

We are grateful to H. Neuhäuser for the preparation of alloys and to V.G. Simkin and S.V. Sumnikov for their assistance in the neutron diffraction experiments performed at the IBR-2 neutron source (Joint Institute for Nuclear Research, Dubna).

FUNDING

This work was supported by the Russian Foundation for Basic Research (project nos. 18-02-00325 and 17-52-44024).

REFERENCES

1. A. J. C. Wilson, Proc. R. Soc. London, Ser. A **181**, 360 (1943).
2. B. E. Warren, *X-Ray Diffraction* (Addison Wesley, New York, 1969).
3. V. I. Iveronova and G. P. Revkevich, *Theory* of *X-Ray Scattering* (Mosk. Gos. Univ., Moscow, 1978) [in Russian].
4. P. Scardi, *Powder Diffraction. Theory and Practice* (RSC, Cambridge, 2008).
5. M. Greenholz and A. Kidron, Acta Crystallogr., Sect. A **26**, 306 (1970).
6. H. Warlimont and G. Thomas, Metal. Sci. J. **4**, 47 (1970).
7. D. Watanabe, H. Morita, H. Saito, and S. Ogawa, J. Phys. Soc. Jpn. **29**, 722 (1970).
8. K. Shiiyama, H. Ninomiya, and T. Eguchi, *Research of Pattern Formation* (KTK Sci., Tokyo, 1994), p. 411.
9. J. M. Ziman, *Models of Disorder. The Theoretical Physics of Homogeneously Disordered Systems* (Cambridge Univ. Press, Cambridge, 1979).
10. A. M. Balagurov, I. A. Bobrikov, B. Mukhametuly, S. V. Sumnikov, and I. S. Golovin, JETP Lett. **104**, 539 (2016).
11. A. M. Balagurov, I. A. Bobrikov, S. V. Sumnikov, and I. S. Golovin, Acta Mater. **153**, 45 (2018).
12. A. M. Balagurov, I. A. Bobrikov, G. D. Bokuchava, V. V. Zhuravlev, and V. G. Simkin, Phys. Part. Nucl. **46**, 249 (2015).
13. A. J. Bradley and A. H. Jay, Proc. R. Soc. London, Ser. A **136**, 210 (1932).
14. O. Kubaschewski, *Iron—Binary Phase Diagrams* (Springer, Berlin, 1982).
15. A. Taylor and R. M. Jones, J. Phys. Chem. Solids **6**, 16 (1958).
16. R. W. Chan, Intermetallics **7**, 1089 (1999).
17. M. V. Matunina, M. A. Zagrebin, V. V. Sokolovskiy, O. O. Pavlukhina, V. D. Buchelnikov, A. M. Balagurov, and I. S. Golovin, Phase Trans. **92**, 101 (2019).

Translated by K. Kugel